Fourier optical route toward multimodal differential microscopy

Jeeban Kumar Nayak,[1,2,*] Niladri Modak,[1,3] Sayan Ghosh,[1] Olivier J.F. Martin,[2] and Nirmalya Ghosh[1]

[1] *Department of Physical Sciences, Indian Institute of Science Education and Research Kolkata, Mohanpur 741246, India*

[2] *Nanophotonics and Metrology Laboratory (NAM), Swiss Federal Institute of Technology Lausanne (EPFL), Lausanne 1015, Switzerland*

[3] *Tampere University, Photonics Laboratory, Physics Unit, Tampere FI-33720, Finland*

(Received 20 September 2025; revised 2 February 2026; accepted 16 March 2026; published 28 April 2026)

We experimentally demonstrate a differential microscopy methodology that facilitates simultaneous amplitude, phase, and differential polarization imaging. The proposed optical spatial differentiator is obtained in a remarkably simple setup by placing a glass cover slip, acting as a signum phase mask in the Fourier plane of a standard $4f$ imaging arrangement. Unlike conventional approaches, the scheme operates without polarized illumination, thereby enabling polarization to serve as an additional contrast within the framework of differential imaging, which facilitates concurrent probing of the phase and polarization gradient information throughout an object. Moreover, the proposed scheme is fully adapted to standard high-resolution microscopy and functions efficiently across a broad wavelength range. The demonstrated simple, low-cost, multifunctional optical spatial differentiator can be easily integrated with conventional bright-field microscopes. It is expected to impact the future of label-free microscopy and optical image-processing techniques, with potential applications in biomedical research, materials science, and several other disciplines.

DOI: 10.1103/97rx-3lx9

I. INTRODUCTION

The amplitude, phase, and polarization degrees of freedom of light have traditionally served as intrinsic mechanisms for image contrast in optical imaging and microscopy [1–5]. The earlier issue of visualizing weakly absorbing or scattering objects was initially addressed by first-generation phase imaging techniques such as phase contrast [6–9] and differential interference contrast (DIC) microscopy [10,11]. These microscopy methods transform the phase distribution within an object into an intensity distribution, enabling the formation of high-contrast images of pure phase objects. In addition to phase, polarization has also been used as an essential contrast mechanism because many natural objects possess intrinsic polarization-anisotropy effects (birefringence and dichroism) due to their anisotropic molecular or structural organization [3,12–14]. These anisotropy effects, once quantified and mapped with desirable spatial resolution, may yield a wealth of morphological, structural, and functional information of potential importance [3,15,16]. Accordingly, polarization imaging holds a distinctive position in label-free optical microscopy and is of significant importance in diverse fields ranging from materials science and biomedical research to metrology [3,15,17].

Despite its potential, traditional polarization imaging techniques struggle to detect subtle morphological variations present in an object due to their limited ability to quantify weak spatial variations in polarization anisotropy effects [3]. Thus, there is a need to develop an imaging technique that can transform a polarization gradient into a corresponding intensity distribution, thereby producing differential polarization-contrast images. To achieve this, the polarization degree of freedom needs to be included as a degree of contrast in the framework of differential imaging; however, most of the existing differential imaging techniques do not accommodate this integration [10,18–21], as they primarily use the polarization of light as a tool to obtain the spatial differentiation [10,18–21].

In this context, it is pertinent to note that there has been significant recent interest in developing miniaturized differential imaging methods to replace conventional bulky quantitative phase imaging setups [18,21–27], and to serve as efficient image processing techniques [20,28,29]. Exploiting the multifunctionality of nanostructures with or without the $4f$ imaging arrangement, optical spatial differentiation is achieved [18–20,30–33]; however, these approaches still require polarized light for spatial differentiation. While some other studies have explored

*Contact author: jeeban.nayak@epfl.ch

differential imaging via Fourier filtering, the potential for integrating polarization and differential imaging remains largely unexplored [34–36].

In this work, we present a unified differential imaging approach that facilitates simultaneous amplitude, phase, and quantitative polarization imaging in a simple experimental system. The optical spatial differentiator achieved in our scheme is realized by placing a glass cover slip as a signum phase mask in the Fourier plane of a conventional $4f$ imaging arrangement; it is hence termed the signum phase mask differential (SPMD) approach. Unlike most existing methods, the SPMD scheme does not need polarized light or the acquisition of multiple images to obtain spatial differentiation. Avoiding these conventional strategies reduces complexity and, more importantly, permits the inclusion of polarization as an additional contrast mechanism in the domain of differential microscopy. As a result, the SPMD imaging approach enables simultaneous probing of differential amplitude, phase, and polarization information within an object. Furthermore, the differentiator performs robustly with high-numerical-aperture (high-NA) objectives across a broad wavelength range, establishing the SPMD method as a cost-effective microscopy platform for real-time label-free microscopy.

II. RESULTS

Our experimental setup employs a standard $4f$ imaging system, with a glass coverslip placed at the center of the Fourier plane [37] [Fig. 1(a)]. The cover slip is positioned in such a way that it imparts a phase (ϕ) of π to the negative spatial frequencies ($\phi = \pi : k_y < 0$) and $\phi = 0$ to the positive spatial frequencies ($k_y > 0$) of the input object in Fig. 1(a). Asymmetric phase manipulation with respect to the spatial frequency k_y is achieved by appropriately tilting or rotating the cover slip. In addition, strong scattering at the coverslip edges significantly suppresses the zero-order transmission. As a result, a commercially available glass coverslip functions effectively as a signum phase mask in the Fourier plane. Further details of the coverslip's physical properties and its impact on image contrast are provided in the Supplemental Material (Sec. S1.A).

The field distribution in the image plane can be derived using the convolution theorem by considering the Fourier spectrum of the object $E_{\text{obj}}(k_x, k_y)$ modulated by the signum function [$\text{sgn}(k_y)$]. This modulation leads to the development of a spatial differentiator, wherein the intensity distribution at the image plane is governed by the derivative of the object field:

$$I_{\text{image}}(x', y') = \left|\mathbf{E}_{\text{image}}(x', y')\right|^2 \propto \left| \int \frac{\partial \mathbf{E}_{\text{obj}}(x, y)}{\partial y} \ln|y' - y|\, dy \right|^2 . \quad (1)$$

Here, $\mathbf{E}_{\text{obj}}(x, y)$ represents the electric field at the object plane, and the signum modulation, determined by the positioning of the coverslip, enforces differentiation in the y direction. A detailed mathematical derivation comprehensively describing the origin of the logarithmic terms is provided in the Supplemental Material [38] (Sec. S2.A). In general, the field $\mathbf{E}_{\text{obj}}(x, y)$ encodes the amplitude, phase, and polarization information of an object. Conventional differential imaging techniques often require specific polarization states to obtain spatial differentiation [21,39,40], which limits their ability to probe polarization-dependent features in the object. In contrast, the proposed SPMD method is intrinsically polarization independent and therefore sensitive to the full vectorial (polarization) properties of the input field [see Eq. (1)]. Expressing the object field as a Jones vector $[E_x(x, y)\ E_y(x, y)]^T$ [3,12,41], the framework naturally extends to amplitude, phase, and polarization gradients. Moreover, the theoretical treatment explaining the multimodal imaging capability of the SPMD imaging scheme is provided in the Supplemental Material [38] (Sec. S2.C).

To illustrate the mechanism, consider an object $\mathbf{E}_{\text{obj}}$ with discrete field discontinuities along the direction of differentiation at $y = a_1, a_2, a_3, \ldots, a_n$ (in the $\mathbf{y}$ coordinates). Treating the gradients of these discrete jumps as delta functions $\delta(a_n)$, the intensity distribution at the image plane becomes

$$I_{\text{image}} \propto \left|\ln|y' - a_1| + \ln|y' - a_2| + \ln|y' - a_3| + \cdots + \ln|y' - a_n|\right| . \quad (2)$$

This expression shows that the intensity distribution at the image plane becomes strongly localized at spatial positions corresponding to the object's field discontinuities, with a logarithmic variation. Such behavior underpins the high-contrast imaging achieved with the SPMD scheme. As a first demonstration, we applied the method to a rectangular phase object exhibiting a π phase jump at its boundaries [Fig. 1(b)I,III]. The differential images reveal intensity localization along the y edges [Fig. 1(b)II,IV], with intensity profiles emulating the logarithmic behavior [Fig. 1(b)ii,iv] predicted by Eq. (1) and Eq. (2). Similar results showcasing the differential image formation of arbitrarily shaped amplitude and phase objects are provided in the Supplemental Material [38] (Figs. S2 and S5). While this study focuses on a one-dimensional signum function for experimental simplicity, the approach can be generalized to isotropic (two-dimensional) differentiation. We can vary the direction of spatial differentiation by steering the orientation of the signum phase mask (glass cover slip) and capture the corresponding differential images, as shown in Fig. 1(c). Spatial differentiation along different directions, $\hat{x} + \hat{y}$ and $\hat{x}$ [Fig. 1(c)], is desirably performed, and consequent intensity localization along different edges is observed in the corresponding differential images.

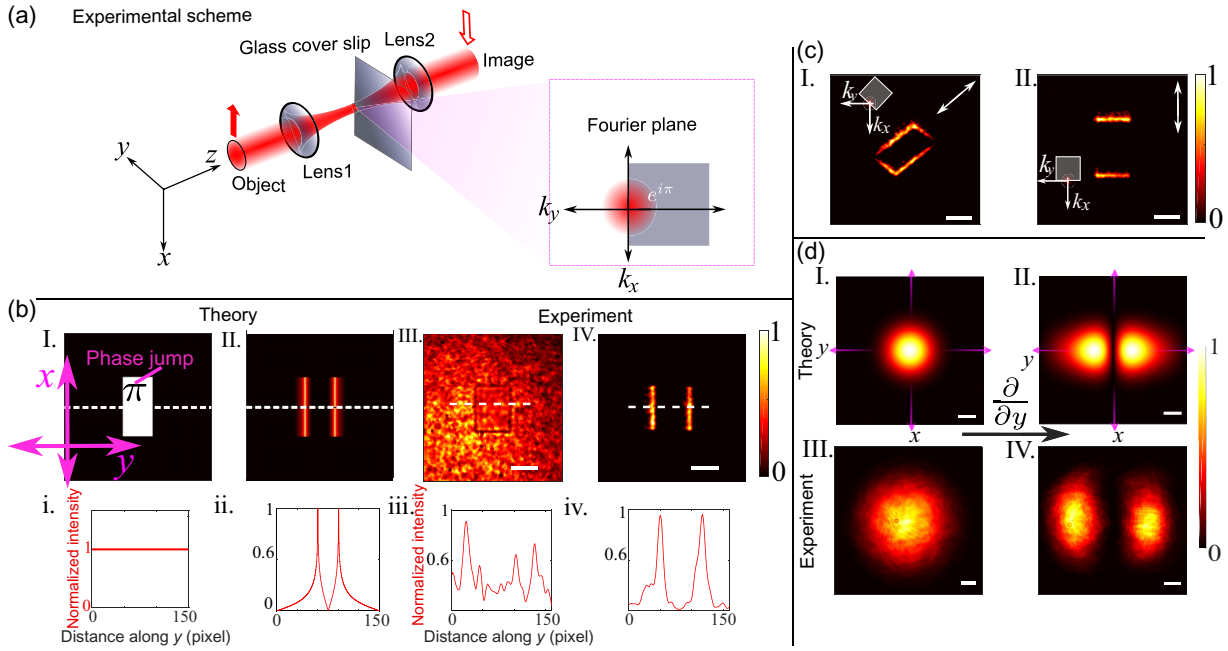

FIG. 1. Working principle of the SPMD imaging methodology. (a) Schematic illustration of the proposed SPMD experimental configuration. A glass cover slip appropriately positioned at the center of the Fourier plane of a $4f$ arrangement acts as a signum phase mask. (b) Both numerically (I, II) and experimentally (III, IV) observed differential images of a rectangular phase object with a phase jump of π at the boundary. (i, ii, iii, iv) Light intensity distribution or line profile in each pixel along the white dashed lines. (c) Differential images of a rectangular phase object with varying directions of spatial differentiation: (I) 45° and (II) vertical ($\hat{x}$) orientations are shown. (d) Spatial differentiation of an input fundamental Gaussian beam (I and II show theoretical results; III and IV show experimental results). The scale bar corresponds to 325 μm.

The SPMD approach is also effective for objects with continuous field variation. This is demonstrated by presenting the numerically and experimentally obtained differential images of an input fundamental Gaussian beam. The differential images feature a two-lobe intensity pattern corresponding to the first-order derivative of the Gaussian function. All phase objects used as imaging targets are prepared using a spatial light modulator (SLM; HOLOEYE LC2012) by modulating the pixels with user-controlled gray-level distributions. A brief description of the phase- and polarization-modulation properties of the SLM is provided in the Supplemental Material [38] (Sec. S1.B). A detailed discussion of the potential influence of the signum phase mask on the spatial resolution of the imaging system is also presented in the Supplemental Material [38] (Sec. S2.B, Fig. S3). It is shown that the true resolution of the imaging system remains unchanged, as the signum phase mask does not suppress or truncate the cutoff spatial frequencies of the optical configuration.

We next demonstrate the adaptability of the SPMD imaging scheme in the realm of microscopy. For this purpose, conventional bright-field microscope objectives are integrated into the existing spatial differentiator setup, and differential images of unstained biological cells are recorded (Fig. 2). Both bright-field and corresponding differential images captured with the SPMD imaging scheme are presented for comparison. For instance, the bright-field image of an onion cell exhibits the expected low contrast due to its weak refractive-index variations and phase-only nature [Fig. 2(a)I,III]. In contrast, the corresponding differential images show a pronounced enhancement in image contrast with clearly visible cellular structures [Fig. 2(a)II,IV]. The corresponding extracted intensity profiles provide further evidence of the improvement in image contrast [Fig. 2(a)III,IV].

To validate the performance of the SPMD imaging approach under high-NA conditions, a differential image of an *Aglaonema commutatum* leaf-cell section is recorded using a 50× microscope objective (NA ≈ 0.8). The resulting images [Fig. 2(b)] clearly reveal internal leaf morphology, including stomata and guard cells. These results provide conclusive evidence that integration of the proposed spatial differentiator with conventional bright-field microscopes holds great potential for real-time label-free imaging of transparent biological objects. Microscope objectives with different magnifications are also used to assess the performance of the SPMD microscope (see Supplemental Material [38], Fig. S5).

We also present a quantitative comparison between the differential images obtained using a commercial DIC microscope and those obtained using the SPMD method, under as similar imaging conditions as possible.

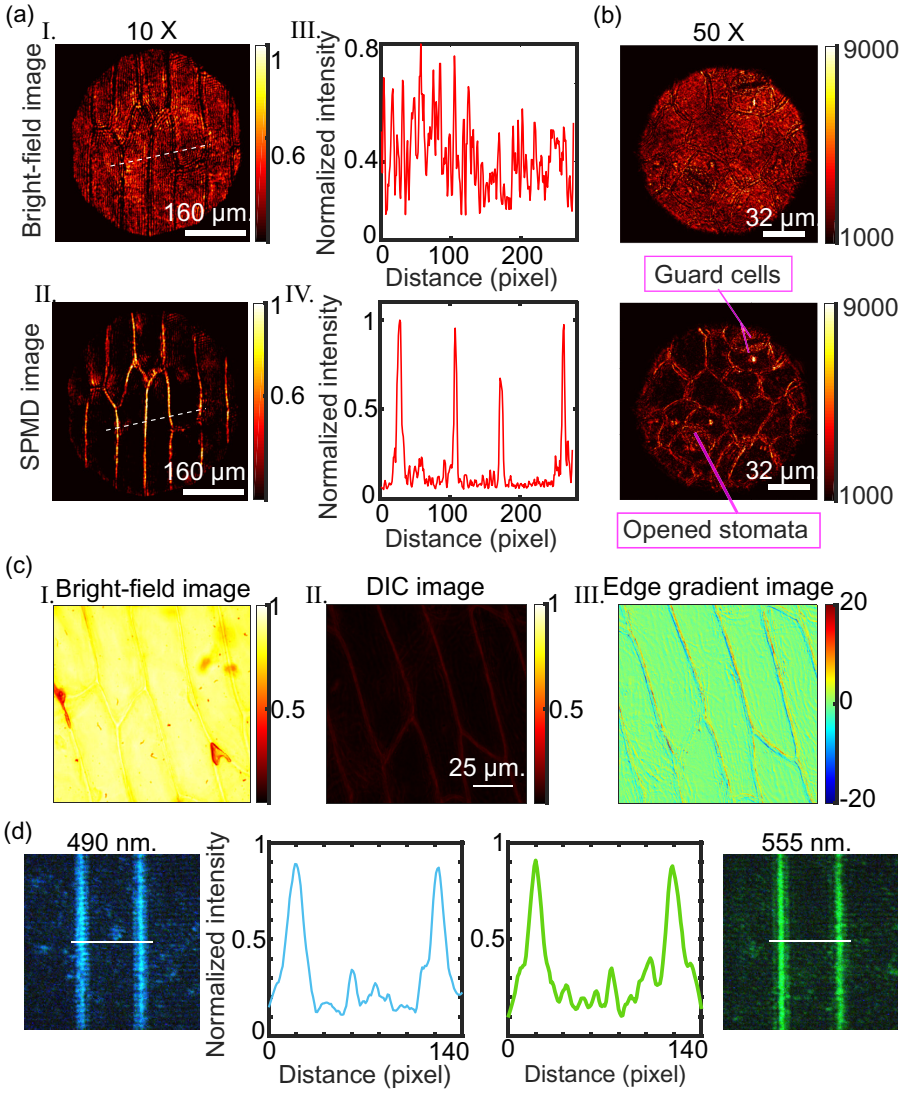

FIG. 2. Adaptation of the signum phase mask differential (SPMD) methodology for microscopy. (a) Bright-field image (I) and the corresponding SPMD-based differential image (II) of an onion cell. Panels (III) and (IV) show the pixel-wise intensity variation along the white dashed lines, highlighting strong intensity localization at the cell boundaries in the case of SPMD imaging. (b) Differential image of a leaf cross section acquired using a 50× microscope objective (NA ≈ 0.8), demonstrating significant contrast enhancement compared to the corresponding bright-field image. (c) Bright-field image (I), and the corresponding differential image (II) of an onion cell obtained using a conventional DIC microscope, shown alongside the extracted edge-gradient image (III). (d) SPMD images of a synthetic phase object recorded at two different illumination wavelengths (490 and 555 nm), together with the corresponding intensity profiles extracted along the white lines indicated in the differential images.

The corresponding results are shown in Fig. 2(c). Two key metrics are chosen for this comparison: (1) the mean edge-gradient magnitude, $(\langle|\nabla I(x,y)|\rangle_{\text{edge}})$, which quantifies edge sharpness in the differential images; and (2) the edge signal-to-noise ratio (SNR), defined as $\text{SNR}_{\text{edge}} = |\nabla I|_{\text{edge}}/\sigma\nabla I_{\text{background}}$, which characterizes edge detectability and is crucial for evaluating differential imaging performance. Onion cells and leaf cells with well-defined cell walls are used as test samples. To calculate $(\langle|\nabla I(x,y)|\rangle_{\text{edge}})$, regions surrounding prominent edges are carefully selected, and the average gradient magnitude over these regions is computed. For the commercial DIC microscope, $(\langle|\nabla I(x,y)|\rangle_{\text{edge}})$ was found to be 6.1, whereas the corresponding value for SPMD images exhibited an enhancement of nearly 2 orders of magnitude, reaching 583.9. This significant difference can be attributed to the distinct illumination schemes employed: SPMD uses coherent laser illumination, while the conventional DIC microscope operates with an incoherent incandescent source. To account for this difference, the edge SNR serves as a more appropriate comparative metric, as both signal and noise gradients are similarly amplified under

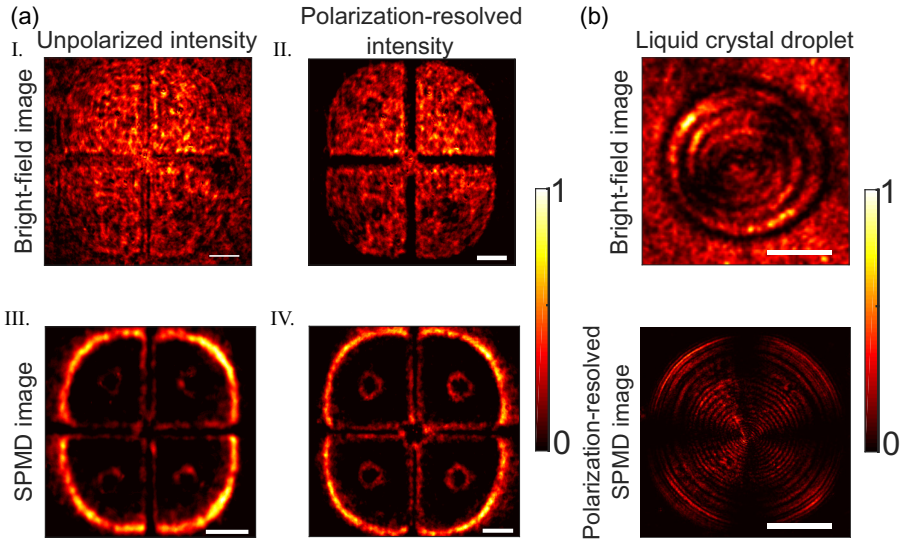

FIG. 3. Inclusion of polarization as an additional degree of contrast in the domain of differential imaging. (a) Unpolarized (I, III) and polarized (II, IV) differential (III, IV), and bright-field (I, II) images of a phase-polarization object. (b) Polarization-resolved differential image of a liquid-crystal droplet reveals the structural orientation of the liquid crystals within. The scale bars in (a) and (b) correspond to 325 and 800 μm, respectively.

coherent illumination. The standard deviation of the noise $\sigma = \sigma_{\text{background}}$ is estimated from homogeneous regions between cell walls. Using this metric, the edge SNR values are found to be comparable for both techniques, yielding 7.2 for DIC and 7.1 for SPMD. These results demonstrate that SPMD provides differential image contrast and edge detectability comparable to conventional DIC microscopy, while offering additional multimodal capabilities.

Furthermore, since the spatial differentiation implemented in the proposed approach is inherently wavelength independent, the same setup can be employed over a broad spectral range. To demonstrate this capability, multiwavelength differential imaging is performed by recording differential images of simple phase objects similar to those shown in Fig. 1(b). The recorded differential images and the corresponding extracted line profiles at wavelengths of 490 and 555 nm [Fig. 2(d)] explicitly demonstrate the broadband performance of the SPMD imaging scheme.

Having established differential image formation for both phase and amplitude objects, we now highlight the most promising feature of the SPMD method: its ability to incorporate polarization as an additional contrast mechanism within the differential imaging framework. Before proceeding with the demonstration, we note that the proposed differential operation in this study is inherently polarization agnostic, enabling edge enhancement without imposing constraints on the incident polarization state; however, to record polarization-resolved differential images or differential polarization-contrast images, it is essential to incorporate polarizing optical elements such as polarizers and retarders (waveplates) into the existing differential imaging setup. We begin by capturing polarization-resolved differential images of a phase-polarization object, revealing the improvement in image contrast as a result of the added polarization degree of freedom. A synthetic phase–polarization object is constructed using the SLM, which simultaneously modulates both phase and polarization according to programmed gray-level distributions (see Sec. S1.B of the Supplemental Material [38] for the detailed SLM properties). Polarization-resolved intensity images are then recorded using combinations of linear polarizers and quarter-wave plates within the SPMD imaging setup. As shown in Fig. 3(a), the recorded polarization-resolved bright-field image [Fig. 3(a)II] reveals the structural boundary of the object, even in bright-field imaging, by suppressing the background signal. The unpolarized differential image [Fig. 3(a)III] provides partial structural contrast, but the polarization-resolved differential image [Fig. 3(a)IV] shows considerably higher contrast, highlighting internal morphology. A further example is given in Fig. 3(b), where a cross-polarized differential image of a radial liquid-crystal droplet clearly reveals both the radial arrangement and layered texture of the anisotropic liquid crystals. These results confirm that SPMD imaging can simultaneously exploit phase and polarization variations to generate high-contrast images of complex objects exhibiting anisotropic optical properties.

We next explore the ability of the SPMD scheme to provide quantitative differential imaging for both phase and polarization objects. To begin with, consider a pure polarization object—one that modifies the polarization state of light ($\mathbf{E}_{\text{obj}}$) relative to the surrounding background. Among the various anisotropic polarization effects, circular retardance is chosen, as this is exhibited by a wide

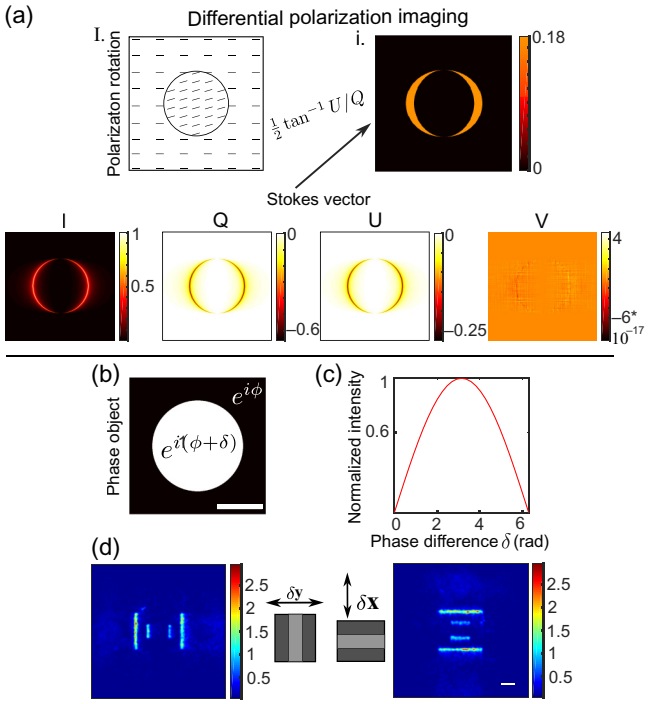

FIG. 4. Demonstration of simultaneous quantitative differential phase and polarization imaging using the SPMD methodology. (a) Quantitative differential polarization-contrast images of a circular polarization object are shown by recording the Stokes vector elements in the image plane. (b),(c) A functional relation between the magnitude of the localized intensity at the image plane and the amount of phase discontinuity (δ) in the object plane is established. (d) Quantitative differential phase images of an object are then constructed using the phase-intensity relation considering spatial differentiation in both the **y** and **x** directions. The scale bars correspond to 400 μm.

range of biological objects, and the shape of the object is kept circular. In this scenario, there is a polarization discontinuity at the boundary of the object, where the polarization angle within the object is rotated by an angle α with respect to the surrounding background [Fig. 4(a)I.]. The SPMD scheme, with its universal differentiation ability, detects this change in polarization and converts it into localized intensity variations, yielding a differential polarization-contrast image [Fig. 4(a)I]. By performing Stokes-vector measurements $[I\ Q\ U\ V]^T$, we retrieve the polarization orientation angle ($=0.5\tan^{-1}(U/Q)$), displaying the quantitative nature of the imaging method [Fig. 4(a)]. A detailed theoretical framework for quantitative polarization-anisotropy analysis is provided in the Supplemental Material [38] (Sec. S2.C, Fig. S4). Furthermore, full (4×4) Mueller matrix measurements and their inverse analysis within the same experimental framework of SPMD imaging are also warranted and are discussed in the Supplemental Material [38] (Sec. S4, Fig. S7).

Finally, we discuss quantitative differential phase (δ) imaging. In the proposed SPMD approach, the localized intensity at the output (image) plane is governed by the spatial gradient of the electric field at the input (object) plane, a characteristic shared with conventional differential phase-contrast techniques. This relationship enables the extraction of quantitative phase information from intensity variations at the image plane. To calibrate this relation, we systematically vary the magnitude of the phase discontinuity at the object plane [Figs. 4(b) and 4(c)] and record the corresponding localized intensity at the image plane. The resulting data is used to construct an intensity-phase calibration curve, which is then fitted using a polynomial function to establish a quantitative mapping between localized intensity and phase discontinuity δ. This calibrated relation is subsequently applied to estimate local phase changes in arbitrary unknown phase objects.

An experimental demonstration of this quantitative differential phase imaging capability is shown in Fig. 4(d), where a phase object is generated using an SLM. The phase discontinuities at the boundaries of the inner and outer rectangular regions are quantitatively extracted from the localized intensity measured at the corresponding edges. Here, we also note that the derived phase images in the case of SPMD imaging do not provide a phase-gradient image of an object as in conventional differential imaging systems. Instead, it provides the phase jump around the boundaries. Further discussion of the nature of the polynomial fitting, as well as supporting theoretical results demonstrating quantitative differential image formation using the SPMD scheme, is provided in the Supplemental Material [38] (Sec. S5, Fig. S8).

III. CONCLUSIONS

In summary, we have demonstrated a low-cost and compact multimodal differential microscopy technique that employs a simple glass cover slip as a signum phase mask within a standard $4f$ imaging system. This approach simplifies differential phase imaging by eliminating the need for polarized illumination and the acquisition of multiple images, while simultaneously enabling polarization to serve as an additional contrast modality in differential microscopy. As a result, our method achieves simultaneous quantitative differential phase and polarization imaging within a single-shot framework. The SPMD technique facilitates amplitude, phase, and quantitative differential polarization imaging in a simple setup. It easily integrates with high-resolution microscopy platforms and operates effectively over a broad wavelength range. It therefore paves the way for cost-effective, multifunctional differential imaging techniques, with promising applications in label-free microscopy.

ACKNOWLEDGMENTS

The authors acknowledge the support of the Indian Institute of Science Education and Research (IISER) Kolkata, an autonomous institute under the Ministry of Education (MOE), Govt. of India. Funding from the Anusandhan National Research Foundation (ANRF) and Scientific and Useful Profound Research Advancement (SUPRA) under Project No. 2023/000451 is gratefully acknowledged.

The authors declare no conflict of interests.

DATA AVAILABILITY

The data that support the findings of this article are not publicly available. The data are available from the authors upon reasonable request.

[1] J. Mertz, *Introduction to Optical Microscopy* (Cambridge University Press, Cambridge, 2019).
[2] D. Evanko, A. Heinrichs, and C. Rosenthal, Milestones in light microscopy, Nat. Cell Biol. **11**, S5 (2009).
[3] C. He, H. He, J. Chang, B. Chen, H. Ma, and M. J. Booth, Polarisation optics for biomedical and clinical applications: A review, Light: Sci. Appl. **10**, 194 (2021).
[4] S.-M. Guo, L.-H. Yeh, J. Folkesson, I. E. Ivanov, A. P. Krishnan, M. G. Keefe, E. Hashemi, D. Shin, B. B. Chhun, N. H. Cho *et al.*, Revealing architectural order with quantitative label-free imaging and deep learning, eLife **9**, e55502 (2020).
[5] L. Mennel, M. M. Furchi, S. Wachter, M. Paur, D. K. Polyushkin, and T. Mueller, Optical imaging of strain in two-dimensional crystals, Nat. Commun. **9**, 516 (2018).
[6] F. Zernike, Diffraction theory of the knife-edge test and its improved form, the phase-contrast method, Mon. Not. R. Astron. Soc. **94**, 377 (1934).
[7] F. Zernike, Phase contrast, a new method for the microscopic observation of transparent objects, Physica **9**, 686 (1942).
[8] C. R. Burch and J. P. P. Stock, Phase-contrast microscopy, J. Sci. Instrum. **19**, 71 (1942).
[9] L. C. Martin, Phase-contrast methods in microscopy, Nature **159**, 827 (1947).
[10] G. Nomarski, Dispositif interférentiel à polarisation pour l'étude des objets transparents ou opaques appartenant à la classe des objets de phase, Patent FR **1**, 124 (1954).
[11] M. Françon, Polarization apparatus for interference microscopy and macroscopy of isotropic transparent objects, J. Opt. Soc. Am. **47**, 528 (1957).
[12] R. A. Chipman, W. S. T. Lam, and G. Young, *Polarized Light and Optical Systems* (CRC Press, Boca Raton, Florida, 2018).
[13] D. H. Goldstein, *Polarized Light* (CRC Press, Boca Raton, Florida, 2017).
[14] J. J. Gil and R. Ossikovski, *Polarized Light and the Mueller Matrix Approach* (CRC Press, Boca Raton, Florida, 2022).
[15] N. Ghosh and I. A. Vitkin, Tissue polarimetry: Concepts, challenges, applications, and outlook, J. Biomed. Opt. **16**, 110801 (2011).
[16] B. Ghosh and K. Agarwal, Viewing life without labels under optical microscopes, Commun. Biol. **6**, 559 (2023).
[17] S. Bhunia, S. Chandel, S. K. Karan, S. Dey, A. Tiwari, S. Das, N. Kumar, R. Chowdhury, S. Mondal, I. Ghosh *et al.*, Autonomous self-repair in piezoelectric molecular crystals, Science **373**, 321 (2021).
[18] H. Kwon, E. Arbabi, S. M. Kamali, M. Faraji-Dana, and A. Faraon, Single-shot quantitative phase gradient microscopy using a system of multifunctional metasurfaces, Nat. Photonics **14**, 109 (2020).
[19] J. Zhou, Q. Wu, J. Zhao, C. Posner, M. Lei, G. Chen, J. Zhang, and Z. Liu, Fourier optical spin splitting microscopy, Phys. Rev. Lett. **129**, 020801 (2022).
[20] M. Cotrufo, A. Arora, S. Singh, and A. Alù, Dispersion engineered metasurfaces for broadband, high-NA, high-efficiency, dual-polarization analog image processing, Nat. Commun. **14**, 7078 (2023).
[21] Y. Shou, J. Liu, and H. Luo, When optical microscopy meets all-optical analog computing: A brief review, Front. Phys. **18**, 42601 (2023).
[22] R. Wang, S. He, and H. Luo, Photonic spin-Hall differential microscopy, Phys. Rev. Appl. **18**, 044016 (2022).
[23] T. Zhu, Y. Lou, Y. Zhou, J. Zhang, J. Huang, Y. Li, H. Luo, S. Wen, S. Zhu, Q. Gong *et al.*, Generalized spatial differentiation from the spin Hall effect of light and its application in image processing of edge detection, Phys. Rev. Appl. **11**, 034043 (2019).
[24] S. He, J. Zhou, S. Chen, W. Shu, H. Luo, and S. Wen, Wavelength-independent optical fully differential operation based on the spin–orbit interaction of light, APL Photonics **5**, 036105 (2020).
[25] S. He, J. Zhou, S. Chen, W. Shu, H. Luo, and S. Wen, Spatial differential operation and edge detection based on the geometric spin Hall effect of light, Opt. Lett. **45**, 877 (2020).
[26] R. Wang, S. He, S. Chen, and H. Luo, Brewster differential microscopy, Appl. Phys. Lett. **121**, 231103 (2022).
[27] Y. Zhou, H. Zheng, I. I. Kravchenko, and J. Valentine, Flat optics for image differentiation, Nat. Photonics **14**, 316 (2020).
[28] A. Silva, F. Monticone, G. Castaldi, V. Galdi, A. Alù, and N. Engheta, Performing mathematical operations with metamaterials, Science **343**, 160 (2014).
[29] H. Kwon, D. Sounas, A. Cordaro, A. Polman, and A. Alù, Nonlocal metasurfaces for optical signal processing, Phys. Rev. Lett. **121**, 173004 (2018).
[30] J. Zhou, H. Qian, J. Zhao, M. Tang, Q. Wu, M. Lei, H. Luo, S. Wen, S. Chen, and Z. Liu, Two-dimensional optical spatial differentiation and high-contrast imaging, Natl. Sci. Rev. **8**, nwaa176 (2021).
[31] A. Cordaro, H. Kwon, D. Sounas, A. F. Koenderink, A. Alù, and A. Polman, High-index dielectric metasurfaces performing mathematical operations, Nano Lett. **19**, 8418 (2019).
[32] T. Zhu, Y. Zhou, Y. Lou, H. Ye, M. Qiu, Z. Ruan, and S. Fan, Plasmonic computing of spatial differentiation, Nat. Commun. **8**, 15391 (2017).
[33] E. Engay, D. Huo, R. Malureanu, A.-I. Bunea, and A. Lavrinenko, Polarization-dependent all-dielectric metasurface for single-shot quantitative phase imaging, Nano Lett. **21**, 3820 (2021).

[34] J. A. Davis, D. A. Smith, D. E. McNamara, D. M. Cottrell, and J. Campos, Fractional derivatives—analysis and experimental implementation, Appl. Opt. **40**, 5943 (2001).
[35] S. Fürhapter, A. Jesacher, S. Bernet, and M. Ritsch-Marte, Spiral phase contrast imaging in microscopy, Opt. Express **13**, 689 (2005).
[36] T.-C. Poon and K. B. Doh, On the theory of optical Hilbert transform for incoherent objects, Opt. Express **15**, 3006 (2007).
[37] J. W. Goodman and P. Sutton, Introduction to Fourier optics, Quantum Semiclass. Opt.: J. Eur. Opt. Soc. Part B **8**, 1095 (1996).
[38] See Supplemental Material at http://link.aps.org/supplemental/10.1103/97rx-3lx9 for additional details on the theoretical modeling of the proposed full-field optical spatial differentiator, as well as further experimental results demonstrating its capability for polarization-resolved broadband quantitative differential imaging.
[39] M. Pluta, Nomarski's DIC microscopy: A review, Phase Contrast and Differential Interference Contrast Imaging Techniques and Applications **1846**, 10 (1994).
[40] Y. Park, C. Depeursinge, and G. Popescu, Quantitative phase imaging in biomedicine, Nat. Photonics **12**, 578 (2018).
[41] S. D. Gupta, N. Ghosh, and A. Banerjee, *Wave Optics: Basic Concepts and Contemporary Trends* (CRC Press, Boca Raton, Florida, 2015).